Chemical Engineering Journal 338 (2018) 358–368

Contents lists available at ScienceDirect

Chemical Engineering Journal

journal homepage: www.elsevier.com/locate/cej

Simultaneous removal of HCHO and elemental mercury from flue gas over Co-Ce oxides supported on activated coke impregnated by sulfuric acid

Jiaqiang Chen[a,b], Caiting Li[a,b,*], Shanhong Li[a,b], Pei Lu[c], Lei Gao[a,b], Xueyu Du[a,b], Yaoyao Yi[a,b]

[a] College of Environmental Science and Engineering, Hunan University, Changsha 410082, PR China
[b] Key Laboratory of Environmental Biology and Pollution Control (Hunan University), Ministry of Education, Changsha 410082, PR China
[c] School of Civil and Environmental Engineering, University of Science and Technology Beijing, Beijing 100083, PR China

HIGHLIGHTS

- The removal efficiency of HCHO and Hg^0 with cobalt-base catalysts supported on ACs was studied.
- The interaction between Hg^0 and HCHO removal was carried out.
- HgO and CO_2 were the main reaction products in the Hg^0 and HCHO removal process respectively.
- The mechanism of simultaneous removal of Hg^0 and HCHO was reasonably speculated.

GRAPHICAL ABSTRACT

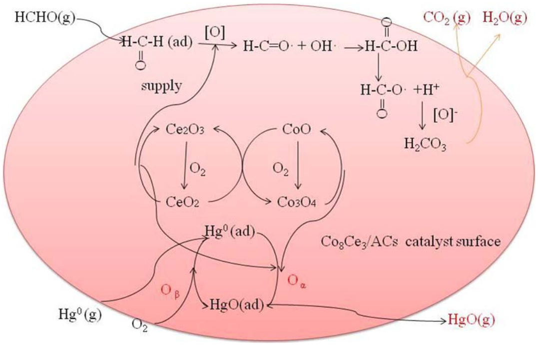

ARTICLE INFO

Keywords:
Elemental mercury
Formaldehyde
Co_3O_4-CeO_2
Activated coke
Catalytic oxidation

ABSTRACT

To obtain a suitable catalyst for simultaneous removal of mercury and HCHO from waste flue gas, we prepared and investigated CoOx-CeO_2 loaded on commercial activated coke granules treated with sulfate acid by impregnation method to remove the two toxic gases. The results revealed that the removal efficiencies of Hg^0 and HCHO over Co_8Ce_3/ACs catalyst were 69.43% and 71.07% respectively in the presence of N_2 and 6% O_2 at 190 °C. And the presence of Hg^0 had little impact on HCHO removal, but formaldehyde had a certain effect on Hg^0 removal. In addition, the effects of individual flue gas component including O_2, NO, SO_2 and H_2O on Hg^0 and HCHO simultaneous removal performance over Co_8Ce_3/ACs catalyst were researched. The physicochemical properties of catalysts were characterized using BET, SEM, XRD, XPS, H_2-TPR and FTIR. By analyzing these characterization results, it was found that the good removal property of the Co_8Ce_3/ACs catalyst was connected with good texture property, high dispersion of cobalt species and strong redox ability. Besides, the interaction between Co and Ce oxides phases could enhance the mobility of active oxygen species, which greatly improved the removal efficiencies of Hg0 and HCHO. Combined with the experiment and characterization results, end products of Hg^0 and HCHO are mainly HgO, CO_2 and H_2O, respectively. So the mechanisms for simultaneous removal of mercury and HCHO were proposed. Of course, the Co_8Ce_3/ACs catalyst would be still modified to achieve the goal of practical industrial application.

---

[*] Corresponding author at: College of Environmental Science and Engineering, Hunan University, Changsha 410082, PR China.
E-mail address: ctli@hnu.edu.cn (C. Li).

https://doi.org/10.1016/j.cej.2018.01.043
Received 14 October 2017; Received in revised form 24 December 2017; Accepted 7 January 2018

1. Introduction

Coal combustion is a major anthropogenic emission source of pollution, which produces NO_X, SO_X, elemental mercury (Hg^0) and VOC_S [1–3]. As far as we know, NO_X and SO_X emission control and treatment technologies have been relatively mature and efficient. And in recent years, Hg^0 has received increased attention due to its high toxicity, persistence, volatility, bioaccumulation in the environment [4,5]. VOCS from coal-fired power stations, which mainly consist of aldehydes (formaldehyde and acetaldehyde), aliphatic and aromatic hydrocarbons and chlorinated hydrocarbons [6]. Formaldehyde (HCHO), as the representative volatile organic compound among them, is an incentive of many diseases, long-term exposure to parts per million (ppm) HCHO-containing air concentrations may cause serious health problems even death, it has also strong photochemical activity and can react photochemically with nitrogen oxides [7–10]. Coal combustion is a major emission source of atmospheric pollutants in China, and relevant laws and regulation about mercury and formaldehyde have been also issued to prevent and control environmental pollution ("Emission standards of atmospheric pollutants in coal-fired power plants GB13223-2011 in China" and "Comprehensive emission standards for atmospheric pollutants GB 16297–1996 in China"). Therefore, effective removal of Hg^0 and HCHO from waste gas is urgently needed to meet strict environmental regulations and improve service of human health care.

In general, mercury emitted from coal combustion exists in three primary forms in the flue gas: particle-bound mercury (Hg^p), elemental mercury (Hg^0), and oxidized mercury (Hg^{2+}) [11]. Compared to Hg^0, Hg^{2+} and Hg^p are more chemically reactive, less volatile, and water soluble, which make them much fast deposition in both dry and wet processes. Therefore, Hg^p and Hg^{2+} can be easily removed by dust control devices like electrostatic precipitator (ESP) or fabric filter (FF) and the wet scrubber like wet flue gas desulfurization (WFGD) [12,13]. And yet, Hg^0 is difficult to be directly removed by existing air pollution control devices. Therefore, the oxidation of Hg^0 to Hg^{2+} followed by the dust control devices and/or wet scrubbing processes becomes a promising method for mercury removal. To date, many methods have been investigated to control HCHO and Hg^0 emissions respectively from flue gas [4,10,14–17]. Among them, catalytic oxidation is a promising and ideal way for HCHO removal, since it can directly convert HCHO to CO_2 and H_2O with simple operation, high removal efficiency, wide application scope, and no secondary pollutants [7,10]. However, the separate HCHO and Hg^0 control technology could result in large equipment investment, high operation cost and other possible problems. Hence, the cost-effective method that can simultaneously remove HCHO and Hg^0 urgently need to be researched. Obviously, catalytic oxidation is the most ideal and effective method to remove HCHO and Hg^0 simultaneously.

Up to present, the catalytic materials for Hg^0 and HCHO oxidation have been developed, mainly the supported noble-metal and transition-metal oxide catalysts, such as Pt/TiO_2 [18], Pt/AlOOH [17], CeO_2-TiO_2 [19], MnOx-Co_3O_4-CeO_2 [8], MnOx [20], Co_3O_4 [21], CoOx-CeO_2/AC [22], CuO-CeO_2/AC [7]. However, the widespread industrial application of noble-metal based catalysts is restricted because of their high costs, poor thermal stability at high temperature, and easy sintering. On the contrary, transition-metal oxide catalysts are more plentiful and cheaper, so they have potential extensive applications in Hg^0 and HCHO oxidation with good thermal stabilities and activities. In the past research, cobalt-base catalysts have been reported to have high activity for Hg^0 and HCHO oxidation separately [21,23–27]. Activated coke (AC) could withstand abrasion and crushing during the circulation and treating process due to its high mechanical strength, compared to conventional activated carbon. But virgin AC presents poor Hg^0 and HCHO removal ability. Previous research has shown that AC treated by acid has higher removal efficiency on Hg^0 [28], oxidative acid could react with surface carbon-based substances and thus the structure of AC could be modified with the addition of oxygen-containing groups of acidic or alkaline, which could improve the adsorption ability of sorbents. Consequently, we used different chemical reagents to modify the original active coke virgin AC for removing HCHO. Through the preliminary experiment, we chose the active coke impregnated by sulfuric acid as the support for formal experiments.

In this paper, a series of cobalt-base catalysts supported on AC impregnated by H_2SO_4 were prepared to investigate systematically their removal performances for Hg^0 and HCHO simultaneously. Aiming to find out a higher removal efficiency catalyst under different conditions, the effects of reaction temperature (110–310 °C), molar ratio and individual flue gas components on Hg^0 and HCHO removal efficiencies were studied as well. Of course, the catalytic oxidation mechanisms of Hg^0 and HCHO removal simultaneously over the catalysts were researched by the essential analysis and characterization results.

2. Materials and methods

2.1. Samples preparation

The commercial AC (cylindrical granule with diameter 6 mm and length of 7–11 mm) was purchased from Gongyi Zhongya water purification materials Co., Ltd., and the virgin AC was washed with deionized water, and then dried in an electric blast oven at 105 °C for 12 h, subsequently activated by H_2SO_4 of 6 mol/L, finally, washed by deionized water to neutral and dried in an electric blast oven at 105 °C for 12 h, the sample obtained was noted as ACs, which employed as the support.

All the catalysts were prepared by impregnating the ACs with a certain amount of cobalt nitrate ($Co(NO_3)_2{\cdot}6H_2O$) and $M(NO_3)x{\cdot}yH_2O$. After impregnation for 24 h, the samples were dried in a drying oven at 105 °C for 12 h and calcined in an electric tube furnace at 500 °C for 4 h under N_2 atmosphere. The samples were noted as Co_8M_1/ACs (Where "8" refers to total metal oxides mass percentage on the samples,"1" refers to the atom molar ratio of Co/M, M = Ce, Cu, Fe, Mn, Ni), which were investigated the removal performance of mercury and formaldehyde. The Co_8Cex/ACs catalysts were prepared by the same steps mentioned above, where "x" represented the atom molar ratio of Co/Ce (x = 1, 3, 6, 0.5).

2.2. Samples characterization

The Brunauer–Emmett–Teller (BET) surface area, pore volume and average pore diameter of catalysts were measured by N_2 adsorption isotherm using a Micromeritics Tristar II 3020 analyzer (Micromeritics Instrument Crop, USA). The specific surface area was calculated by the N_2 desorption plots of the catalysts.

The scanning electron microscopy (SEM) characterization was carried out on a FEI Quanta 400 FEG apparatus to get the images of the prepared samples.

X-ray diffraction (XRD) measurement was carried out on a Bruker D8 ADVANCE equipped with Cu Kα radiation. The diffraction patterns were collected in a 2θ range of 10–80°.

The X-ray photoelectron spectroscopy (XPS) measurements were performed on a Thermo K-Alpha equipped with Al Kα radiation. The binding energy value of 284.6 eV.

The temperature-programmed reduction of hydrogen (H_2-TPR) measurements were conducted using an AutoChem 2920 automated adsorption analyzer equipped with a TCD detector.

Fourier transform infrared (FTIR) spectra were collected on Iffinity-1 (Shimadzu Japan) spectrometer with a resolution 4 cm^{-1}, and the spectrometer in the frequency range of 4000 and 400 cm^{-1}.

2.3. Mercury and HCHO removal performance tests

All the samples tests were measured in traditional fixed-bed reactor (quartz tube 60 mm i.d.), in which about 20 g sample was used. The

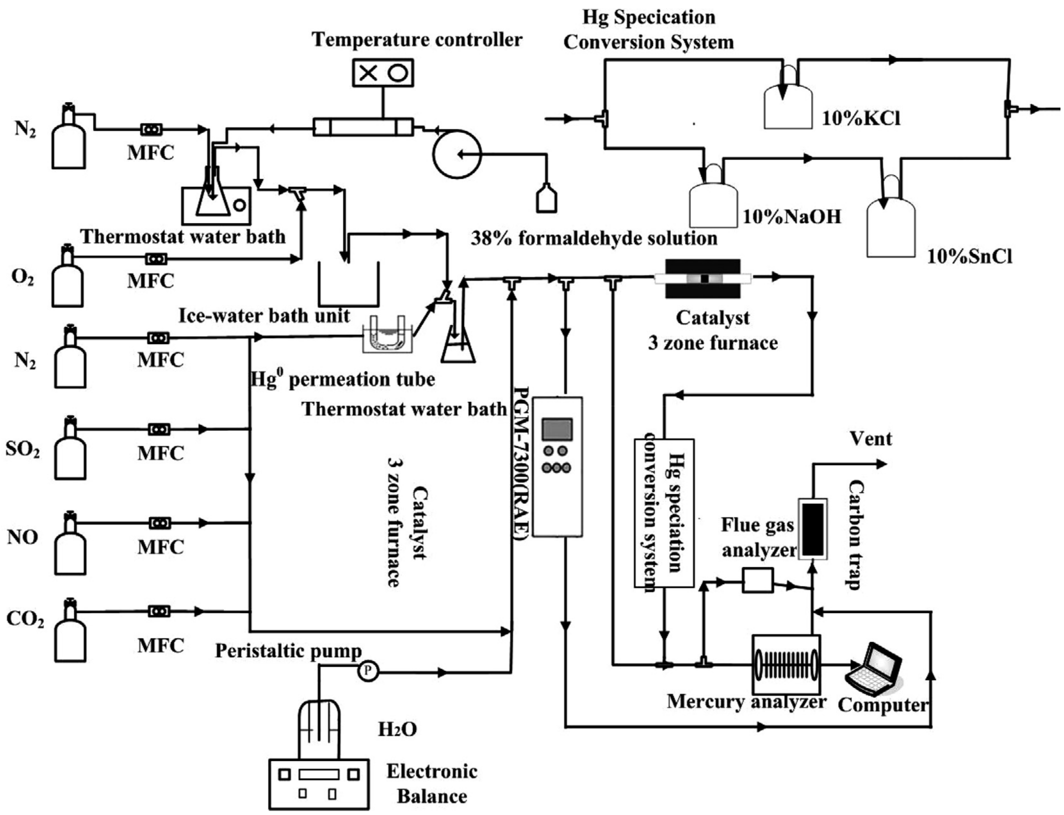

Fig. 1. Schematic diagram of the experimental setup.

reaction feed contained about 100 ppm HCHO, Hg^0 (90 μg/m^3),6 vol% O_2 and pure N_2 as balance, the other gases, such as SO_2, NO, 12% CO_2 and 8% $H_2O(g)$ were added when required. The simulated coal combustion flue gas (denoted as "SFG") used in the experiments was a mixture of 6% O_2, 12% CO_2, 350 ppm NO, 400 ppm SO_2, 8% $H_2O(g)$ and balance N_2. For major experiments, a total gas flow of 500 mL/min (GHSV = about 4000 h^{-1}) was introduced into the fixed-bed reactor at temperatures from 110 to 310 °C. All the flow gas except H_2O were controlled accurately by mass flow controller (MFC, SevenStar Huachuang, China), and the water vapor was generated by injecting water into Teflon tube wrapped with a temperature-controlling heating strip at 110 °C through peristaltic pump. Schematic diagram of the experimental setup is shown in Fig. 1. The experimental process was as follow: the formaldehyde solution (38 wt%) commercially available was transferred by the peristaltic pump into Teflon tube which was wrapped with temperature-controlled heating band (120 °C). A flow of pure N_2 (370 mL/min) used as carrier gas passed through the conical flask that contained the HCHO vapor. Then, it passed through a condensing unite to remove water vapor, and finally mixed with the O_2 (30 mL/min) and mercury vapor in the gas mixing chamber. The gas-phase Hg^0 was generated by a mercury permeation tube (VICI Metronics, USA) and carried into the gas mixing chamber by a flow of pure N_2 (100 mL/min). The inlet gas was monitored after the variation of HCHO concentration less than 5% and mercury concentration was almost constant (90 μg/m^3) .

In each test, about 20 g sample was packed in the quartz tube placed in the middle of the fixed-bed reactor. In our previous work [7,22], the quartz tube and the Teflon tube were proven to have almost no effect on removal performance of mercury and HCHO. The inlet and outlet Hg^0 concentrations were monitored by RA-915 M online mercury analyzer (LUMEX, Russia) with a detection limit of 2 ng/m^3. A mercury speciation conversion system coupled with RA-915 M online mercury analyzer was employed to measure Hg^0 and Hg^{2+}concentrations in the outlet flue gas when it was necessary. The specifications of mercury speciation conversion system are the same as our previous research [22]. The inlet and outlet HCHO concentrations were measured by a PGM-7300(RAE, USA), and CO_2 was detected with PGA-650 (Phymetrix, USA). The content of the flue gas components (NO, SO_2) was monitored by the MRU Infrared Gas Analyzer MGA5 (74172 NSU-Obereisesheim, Germany). All the experiments were carried out three times to reduce experimental error. The gas flow was transferred to the fixed-bed reactor and maintained 3 h. The removal and conversion efficiency of mercury (mercury oxidation and mercury capture) and HCHO were calculated by the following equation:

$$E_{Hg}(\%) = \frac{Hg^0_{in} - Hg^0_{out}}{Hg^0_{in}} \tag{1}$$

$$E_{HCHO}(\%) = \frac{HCHO_{in} - HCHO_{out}}{HCHO_{in}} \tag{2}$$

$$E_{oxi}(\%) = \frac{[Hg]^T_{out} - [Hg]^0_{out}}{[Hg]^0_{in}} \tag{3}$$

$$E_{cap}(\%) = E_{Hg} - E_{oxi} = \frac{[Hg]^0_{in} - [Hg]^T_{out}}{[Hg]^0_{in}} \tag{4}$$

where E_{Hg} and $E_{HCHO,}$ E_{oxi} and E_{cap} represent the efficiency of Hg^0 and HCHO, the efficiency of mercury oxidation and capture respectively. The Hg^0_{in} and Hg^0_{out} represent the Hg^0 concentration (μg/m^3) at the inlet and outlet of the test, respectively, and $[Hg]^T_{out}$ represents the sum of $[Hg]^{2+}_{out}$ and $[Hg]^0_{out.}$ Similarly, $HCHO_{in}$ and $HCHO_{out}$ represent HCHO concentration (ppm) at the inlet and outlet of the test.

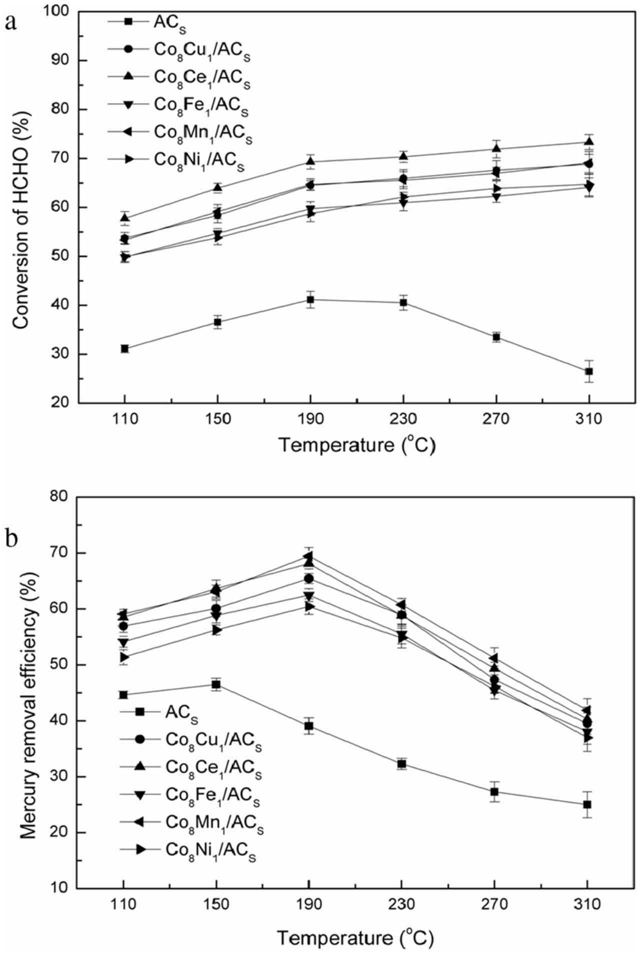

Fig. 2. Simultaneous removal performance of HCHO and Hg^0 over Co_8M_1/ACs catalysts. (Reaction condition: 100 ppm HCHO,90 μg/m^3 Hg^0, 6% O_2 and balance N_2, 20 g sample, total flow rate 500 mL/min).

3. Results and discussion

3.1. Removal performance tests of HCHO and Hg^0

3.1.1. Catalytic activity of Co_8M_1/ACs catalysts

In order to find out the optimal metal oxide additives loaded on the activated coke for simultaneous removal performance of HCHO and Hg^0, a series of experiments were carried out at 110–310 °C, all the metal oxides loading value and the molar ratio of Co/M used in the study were 8% and 1 respectively. As shown in Fig. 2, the Co_8Ce_1/ACs catalyst exhibited the best HCHO removal performance and second-highest Hg^0 removal efficiency, the sequence of catalytic activity for HCHO removal was as follows: Co_8Ce_1/ACs > Co_8Cu_1/ACs > Co_8Mn_1/ACs > Co_8Fe_1/ACs > Co_8Ni_1/ACs > ACs, and the Hg^0 removal performance over the Co_8M_1/ACs catalysts were ordered Co_8Mn_1/ACs > Co_8Ce_1/ACs > Co_8Cu_1/ACs > Co_8Fe_1/ACs > Co_8Ni_1/ACs > ACs. The possible reason is that a certain kind of synergistic effect between cobalt oxide and other transition metal oxide existed over the ACs support. Ceria has large oxygen storage capacity and unique redox cycling between Ce^{3+} and Ce^{4+} [29], which could greatly affect cobalt oxide redox property and it was consistent with H_2-TPR result later, so the Co_8Ce_1/ACs may exhibited better removal efficiency than other samples. Of course, it could be clearly seen that the conversion of formaldehyde gradually increased with the rising of temperature and leveled out finally except ACs, in addition, Hg^0 removal efficiency increased first, but it gradually decreased after it reached max value. At 190 °C, Hg^0 removal efficiency and HCHO conversion were 68.11% and 69.29% respectively. In consideration of operation cost and removal performance in practice, the optimal temperature (190 °C) was set as default operational condition in the following tests.

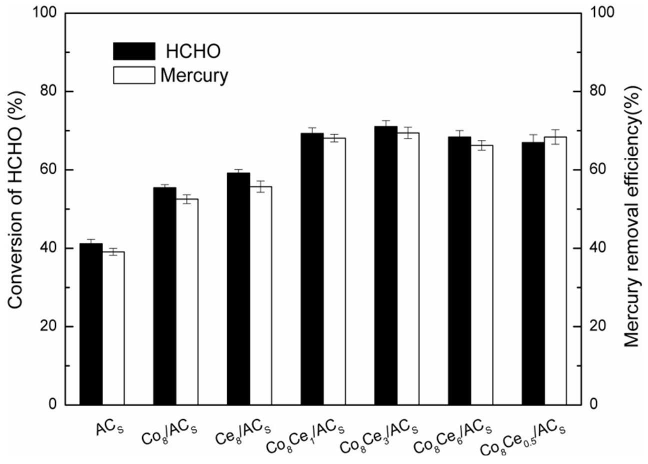

Fig. 3. The effect of Co/Ce molar ratio(x) on removal performance of HCHO and Hg^0 over Co_8Cex/ACs samples. (Reaction condition: 100 ppm HCHO, 90 μg/m^3 Hg^0,6% O_2 and balance N_2, 20 g sample, total flow rate 500 mL/min, reaction temperature 190 °C).

3.1.2. Effect of Co/Ce molar ratio

The HCHO and Hg^0 removal performances over ACs, Co_8/ACs, Ce_8/ACs and Co_8Cex/ACs samples at 190 °C were researched. As shown in Fig. 3, the Co_8Cex/ACs samples displayed better removal abilities of HCHO and Hg^0 than Co_8/ACs and Ce_8/ACs, which indicated a synergistic effect may exist between cobalt oxide and ceria over Co_8Cex/ACs. The addition of CeO_2 could result in an increase on the amount of reducible Co^{3+} and enhance the redox ability of Co_8Cex/ACs by promoting the mobility of adsorbed oxygen species [30,31], which improved the HCHO and Hg^0 removal efficiencies. Furthermore, all the Co_8Cex/ACs catalysts presented excellent efficiencies and their differences were slight, indicating the Co/Ce molar ratio was not a significant influence. Of course, the Co_8Ce_3/ACs showed relatively well removal performance of HCHO and Hg^0, so further studies were developed on the Co_8Ce_3/ACs.

3.2. Interaction between Hg^0 and HCHO removal

3.2.1. Effect of Hg^0 on HCHO conversion

To test and evaluate the removal performance of Co_8Ce_3/ACs catalyst for simultaneous removal of Hg^0 and HCHO, the interaction between Hg^0 and HCHO removal was researched. As shown in Fig. 4(a), HCHO conversion efficiency with or without gas-phase mercury revealed similar trends at 110–310 °C. It was obviously seen that HCHO conversion efficiency improved with the increase of reaction temperature from 110 to 190 °C, and then increased slightly from 230 to 310 °C. In addition, HCHO conversion efficiency was almost same at different temperatures whether gas-phase mercury existed or not, indicating that the addition of Hg^0 had little influence on HCHO conversion. The possible reason may be that the Hg^0 concentration (90 μg/m^3) was very low compared to HCHO concentration (100 ppm).

3.2.2. Effect of HCHO on Hg^0 removal

The effect of HCHO on Hg^0 removal over Co_8Ce_3/ACs catalyst is shown in Fig. 4(b), the results demonstrated the change trend of Hg^0 removal efficiency as a function of reaction temperature was similar at different HCHO concentration, they all increased as the reaction temperature increased to 190 °C, and then gradually decreased. Besides, it was obvious that Hg^0 removal efficiency decreased sharply at all reaction temperatures when HCHO existed, indicating that the presence

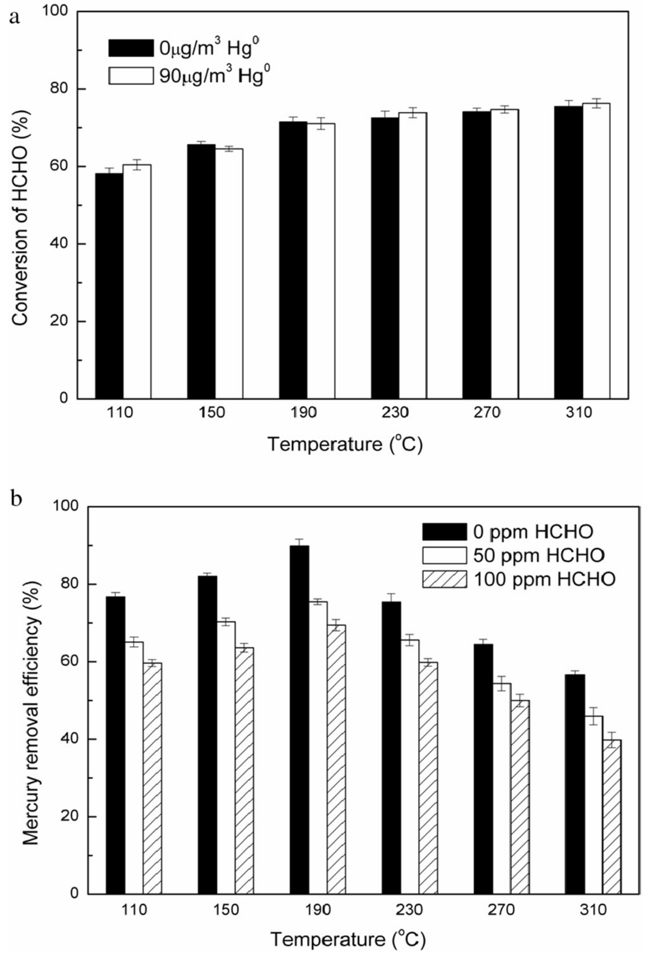

Fig. 4. The interaction between mercury and formaldehyde on Co_8Ce_3/ACs catalyst. (Reaction condition: balance N_2 and 6% O_2, 20 g sample, total flow rate 500 mL/min).

of HCHO could significantly reduce the catalytic activity of Co_8Ce_3/ACs for Hg^0 removal. Of course, it could be seen that the higher HCHO concentration was, and the more obvious inhibitory effect was. The Hg^0 removal efficiency decreased sharply from 89.89% to 69.43% at 190 °C when 100 ppm HCHO was introduced. This may be because HCHO can compete with gas-phase mercury for occupying the surface active sites of catalyst and consuming surface active oxygen, hence leading to a sharp decline in Hg^0 removal efficiency.

3.3. Effect of flue gas components

Fig. 5(a) and (b) showed the effects of flue gas components (O_2, NO, SO_2 and H_2O) for removing Hg^0 and HCHO over Co_8Ce_3/ACs catalyst at 190 °C respectively.

3.3.1. Effect of O_2

As displayed in Fig. 5(a) and (b), O_2 had a significant impact on simultaneous removal of Hg^0 and HCHO as an important flue gas component. It could be clearly seen that the Co_8Ce_3/ACs catalyst revealed poor removal performance for simultaneously elimination of Hg^0 and HCHO under pure N_2, whose removal efficiencies were 30.39% and 35.89% respectively at 190 °C, but when 6% O_2 was introduced, the efficiencies were improved by about 40% and 35% accordingly. Based on the XPS and FTIR results discussed later, the surface oxygen of the catalyst could supply abundant chemisorbed and lattice oxygen, consequently react with adsorbed gas-phase Hg^0 and HCHO. Thus, with the addition of 6% O_2, the gas-phase O_2 could regenerate the consumed lattice oxygen and replenish chemisorbed oxygen to facilitate their removal [32,33]. Further increasing O_2 concentration to 10%, no obvious promotion of Hg^0 and HCHO removal was found, indicating 6% O_2 was sufficient for simultaneous removal of Hg^0 and HCHO. This was consistent with other researches [34,35].

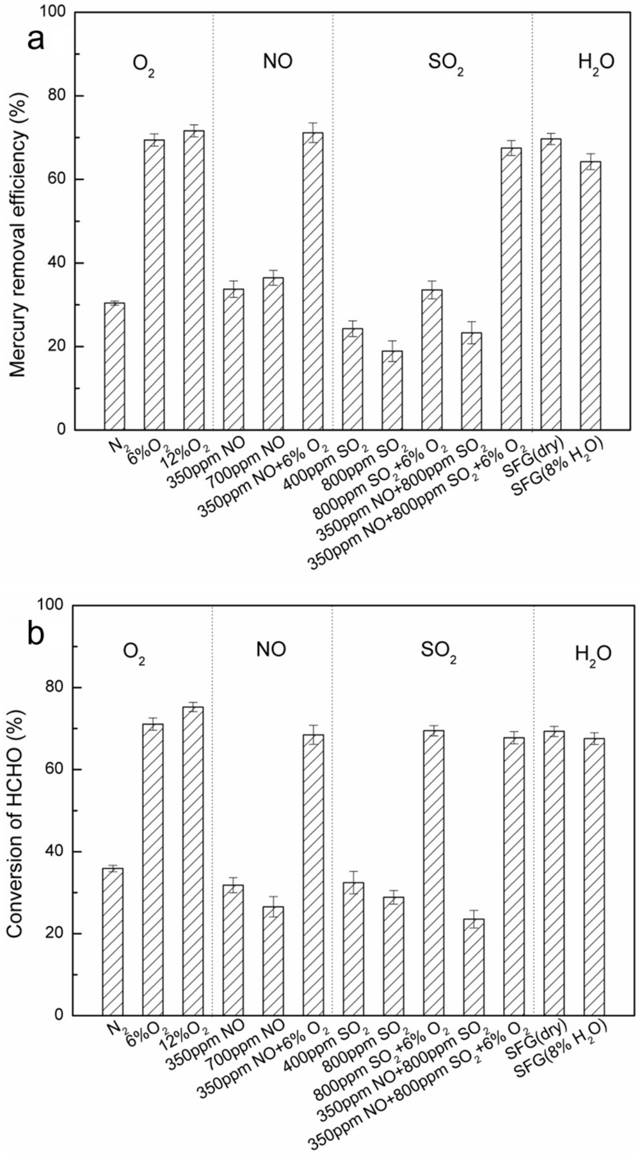

Fig. 5. Effect of flue gas components on HCHO and Hg^0 removal efficiencies over Co_8Cex/ACs catalyst. (Reaction condition: 100 ppm HCHO, 90 μg/m^3 Hg^0, 0–12% O_2, 0–800 ppm SO_2, 0–700 ppm NO, 8% H_2O, 20 g sample, total flow rate 1000 mL/min, reaction temperature 190 °C).

3.3.2. Effect of NO

From Fig. 5(a) and (b), we could see that NO had different effects on removal of Hg^0 and HCHO, the promotional effect on Hg^0 and inhibiting effect on HCHO removal were observed over Co_8Ce_3/ACs at 190 °C respectively. According to the report [36], NO could adsorb on the surface of Co_8Ce_3/ACs to cover active sites and react with labile surface oxygen to facilitate the formation of NO_2, which was consistent with FTIR characterization result later. The reduced surface oxygen could not be supplied timely without O_2, moreover, there existed competitive adsorption between NO and HCHO, therefore, leading to the decrease of HCHO conversion efficiency. And with addition of 6% O_2 into the gas stream, the HCHO conversion efficiency was enhanced from about 40% to 68.48%, which was attributed to the surface oxygen replenished by the additional O_2. However, it had been reported that

NO_2 could improve the Hg^0 oxidation on the surface of catalyst [37], and it was in line with the result from Fig. 5(a). Of course, when 6% O_2 was added into the inlet gas stream, the mercury removal efficiency also significantly increased like the formaldehyde's.

3.3.3. Effect of SO_2

The effect of SO_2 on removal of Hg^0 and HCHO are presented in Fig. 5(a) and (b) respectively. It could be clearly seen that the removal performances of Hg^0 and HCHO were obviously inhibited without O_2. When SO_2 concentration increased from 400 to 800 ppm, the Hg^0 and HCHO removal efficiencies had different degree drop. The phenomenon could be explained by the following aspects; On the one hand, SO_2 could adsorb on the surface of catalyst and occupy the similar active sites, and SO_2 was a small molecular contaminant, it may be more favorable than Hg^0 and HCHO to cover the active sites. On the other hand, SO_2 may react with active components in catalyst to form sulfates, which was consistent with the FTIR result. Besides, with addition of 6% O_2 into the gas stream, the removal efficiencies of Hg^0 and HCHO increased to a varying degree. The Hg^0 and HCHO removal efficiencies were 23.3% and 23.54% respectively when 350 ppm NO and 800 ppm SO_2 were introduced the inlet gas stream balanced in pure N_2. This, which indicated that the coexisted of NO and SO_2 could severely inhibite their removal efficiencies. However, the inhibitory effect was not obvious in the presence of 6% O_2, demonstrating Co_8Ce_3/ACs had good NO and SO_2 durability at optimal temperature (190 °C).

3.3.4. Effect of H_2O

Water vapor existed in coal combustion flue gas and generally had been reported as an inhibiting effect on the removal of Hg^0 [19,22,38]. Likewise, a negative effect of H_2O on the removal of mercury and HCHO was also observed in the experiments. The removal efficiencies of mercury and HCHO all declined to a certain extent with addition of 8% water vapor to the gas stream, which could be interpreted by the competitive adsorption between $H_2O(g)$ and Hg^0 as well as HCHO for active sites on Co_8Ce_3/ACs catalyst. But formaldehyde is hydrophilic, so water steam had smaller impact on formaldehyde. However, the removal efficiencies of mercury and HCHO under SFG (8% H_2O) condition were still higher than under pure N_2, which indicated the promotional effect of O_2 far outweigh the negative effect of H_2O and SO_2.

3.4. Stability of the catalyst and mercury speciation conversion experiment

The stability test results for simultaneous removal of mercury and HCHO as well as mercury speciation conversion experiment over the Co_8Ce_3/ACs catalyst are displayed in Fig. 6(a) and (b) respectively. The stability test of the Co_8Ce_3/ACs continued for 60 h. Apparently, for 3 h prior, the removal efficiencies of HCHO and Hg^0 were instability, and then it showed a slow downward trend and their decline were about 15% to 20%. The reason was probably that adsorption ability of the Co_8Ce_3/AC_S was very good in the first, active sites were slowly occupied and consumed, therefore, the efficiencies dropped gradually and still kept at about 50%, which attributed to the surface active oxygen species could be replenished by the gas-phase O_2. In addition, it was worth noticing that the efficiency of HCHO selectivity conversion to CO_2 was about 95%. The result of Fig. 6(b) indicated Hg^0 oxidation played an important role in the Hg^0 removal process at 110–310 °C. And Hg^0 adsorption occupied a small fraction of removal efficiency, which was consistent with Hg 4f characterization result. At the same time, the result could be certified by Hg^0 removal efficiency in 60 h and over virgin ACs .

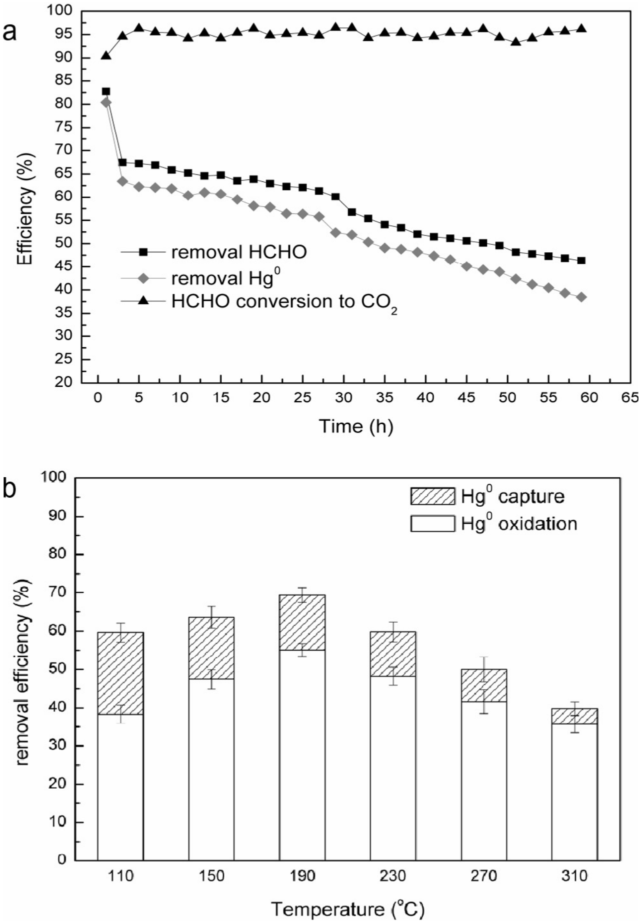

Fig. 6. Stability of the catalyst and mercury speciation conversion experiment. (Reaction condition: (a) 100 ppm HCHO, 90 μg/m^3 Hg^0, SFG, 20 g sample, total flow rate 1000 mL/min, reaction temperature 190 °C. (b) 90 μg/m^3 Hg^0,6% O_2 and balance N_2, 20 g sample, total flow rate 500 mL/min, reaction temperature 110–310 °C).

Table 1
BET specific surface area and pore parameters of the samples.

Samples	BET surface area (m^2/g)	Pore volume (cm^3/g)	Average pore diameter (nm)
ACs	66.69	0.107	6.42
Co_8/ACs	64.91	0.111	6.82
Ce_8/ACs	63.47	0.106	6.13
Co_8Ce_1/ACs	62.55	0.103	6.60
Co_8Ce_3/ACs	62.36	0.096	6.17
Co_8Ce_6/ACs	63.97	0.103	6.44
$Co_8Ce_{0.5}$/ACs	63.07	0.099	6.29

3.5. Characterization of materials

3.5.1. Textural, morphologic, and structural characterizations

The BET specific surface area, pore volumes and average pore diameter of the catalysts are listed in Table 1. It could be clearly observed that the ACs had a similar specific surface with other metal oxide modified catalysts. This demonstrated that Co-Ce mixed oxides were well dispersed on the surface of the ACs support, which was in line with the XRD results. We can see all the samples have not high specific surface area(about 60 m^2/g) compared to other activated carbon, indicating their adsorption capacity were not good, and this was confirmed by the experiments. And removal process of Hg^0 and HCHO mainly depended on catalytic oxidation. In addition, from the results of experiments, the removal performance of Hg^0 and HCHO had no necessary relation to the BET specific surface area.

Fig. 7 presents the SEM images of the prepared samples. It could be seen that the active components were well dispersed on the surface of ACs. One thing to be aware of was that very few agglomerates were observed on the surface of Co_8Ce_x/ACs samples. However, more agglomerates appeared on the surface of Co_8/ACs and Ce_8/ACs, which

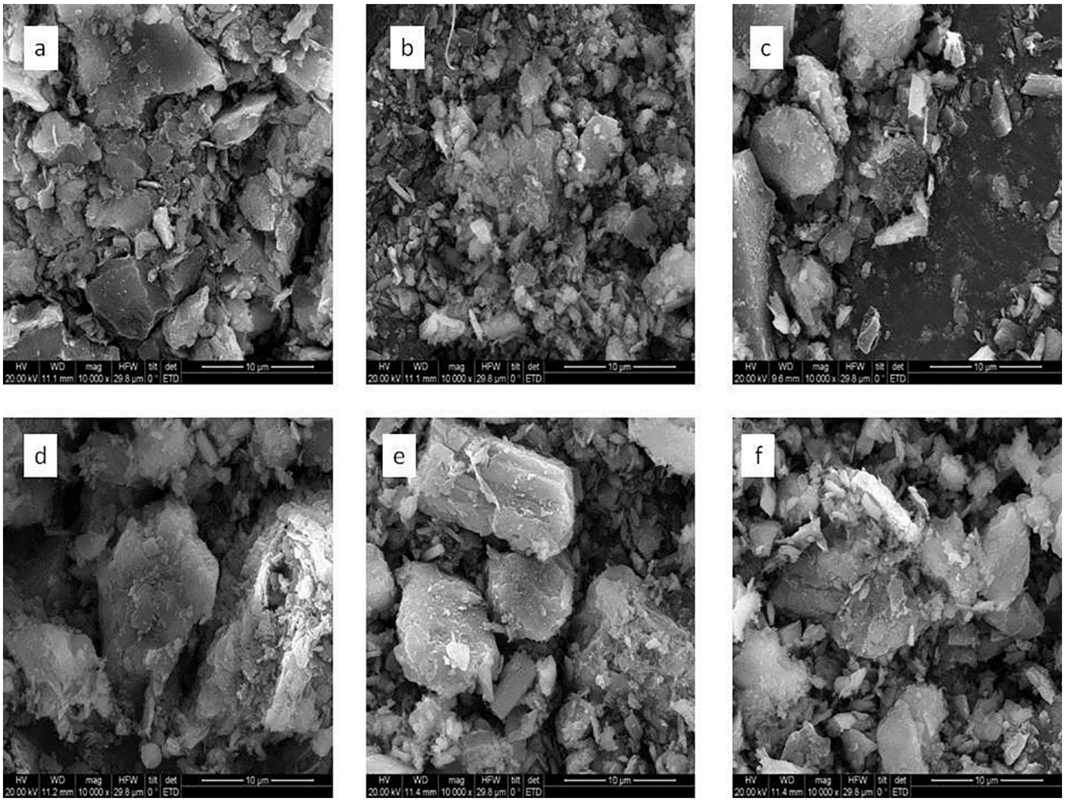

Fig. 7. SEM images of (a) ACs, (b) Co_8/ACs, (c) Ce_8/ACs, (d) Co_8Ce_1/ACs, (e) Co_8Ce_3/ACs, (f) $Co_8Ce_{0.5}$/ACs.

illustrated the dispersion of active components was not good. Meantime, the removal performance of Hg^0 and HCHO over the Co_8/ACs and Ce_8/ACs catalysts was inferior to the Co_8Ce_x/ACs catalysts. So combined with the SEM and latter XRD characterization results, the highly dispersion of active components on the surface of ACs support was beneficial to the removal performance of the catalysts.

To identify the crystal structures of the virgin ACs, Co_8/ACs, Ce_8/ACs and Co_8Ce_3/ACs samples, the XRD measurement was carried out, and the results are presented in Fig. 8. It could be seen that the typical peak of AC was detected at 2θ = 26.60° in the all samples. For the Co_8/ACs sample, the main cobalt specie was Co_3O_4 phase, and its corresponding peaks were observed at 2θ = 31.24°, 65.22°, 74.07° in Co_8/ACs. Moreover, the peaks at 2θ = 42.38° and 61.49° were attributed to CoO phase, which was in line with XPS characterization result. Of course, for the Ce_8/ACs sample, the feature diffraction peaks of CeO_2 at 2θ = 28.65°, 47.45° and 56.32° were detected. However, no obvious characteristic peaks of CeO_2 were observed over Co_8Ce_3/ACs sample, indicating the presence of cobalt oxide was in favor of dispersion of CeO_2 over ACs support. At the same time, the result could be a favorable condition for the efficiency of Hg^0 and HCHO removal.

3.5.2. H_2-TPR

To investigate the redox behavior of the catalysts in the study, the H_2-TPR analysis results of three different samples are shown in Fig. 9.

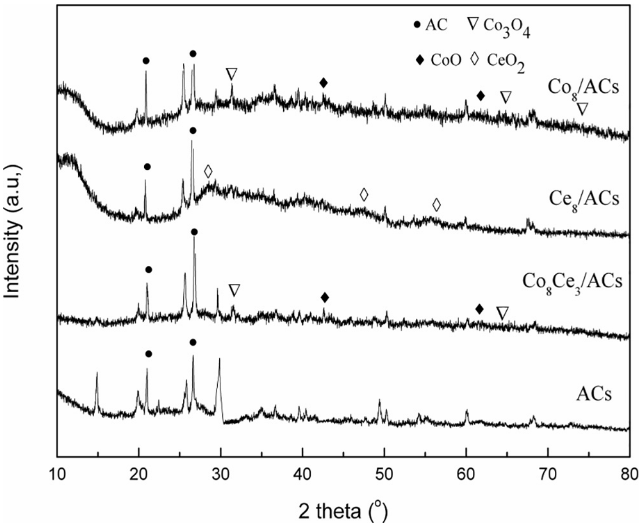

Fig. 8. XRD patterns of the samples(ACs, Co_8/ACs, Ce_8/ACs and Co_8Ce_3/ACs).

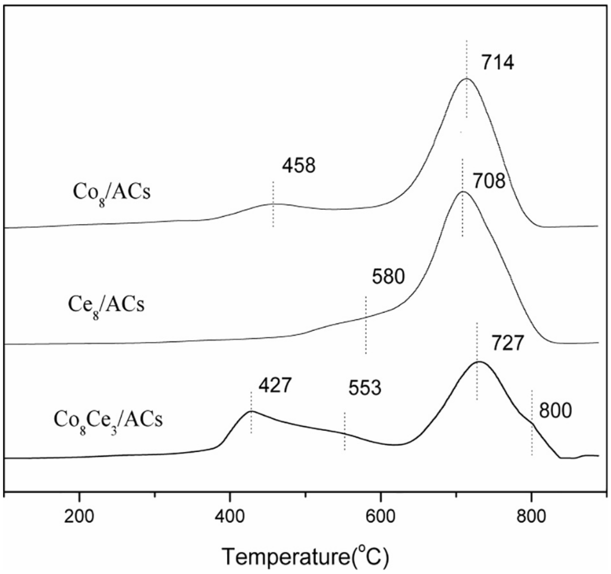

Fig. 9. H_2-TPR profiles of Co_8/ACs, Ce_8/ACs and Co_8Ce_3/ACs.

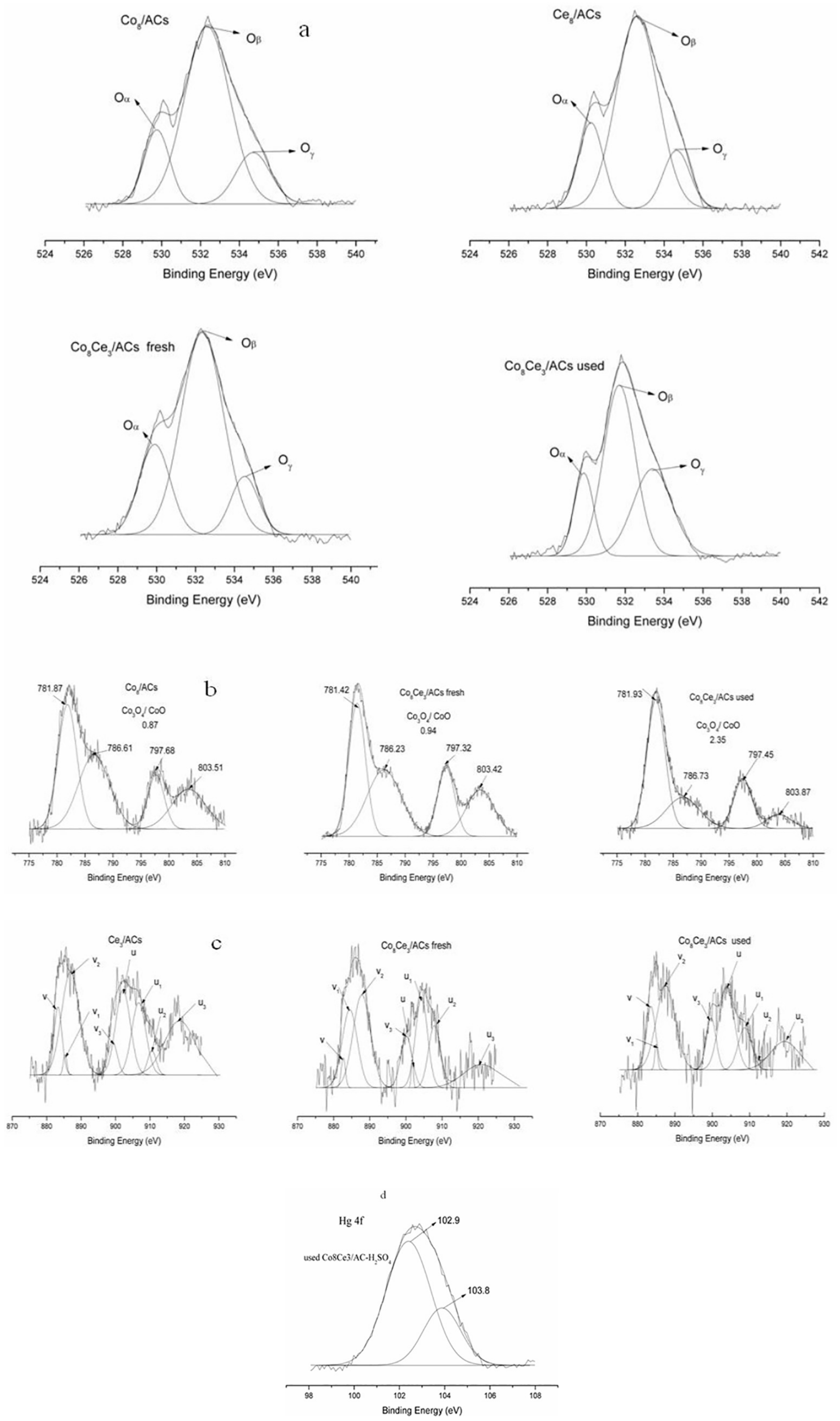

Fig. 10. XPS spectra for O1s, Co2p and Ce3d of the as-prepared samples: (a) O 1s. (b) Co 2p. (c) Ce 3d. (d) Hg 4f.

The reduction of the Ce_8/ACs sample occurred at 580 °C and 708 °C. The one at relatively lower temperature could be assigned to the surface Ce^{4+}, and the higher one was attributed to the bulk oxygen [39]. For Co_8/ACs, there were also two reduction peaks appeared at approximately 458 °C and 714 °C, the peak at 714 °C was attributed to the interaction between solid carbon and H_2, while 458 °C could be assigned to the reduction of Co^{3+} in Co_2O_3 or Co_3O_4 [40,41]. However, for the Co_8Ce_3/ACs catalyst, it could be seen that the reduction of two

Table 2
Elemental contents of Co_8/ACs, Ce_8/ACs, fresh and used Co_8Ce_3/ACs by XPS analysis.

Samples	Ratio of the oxygen			Co_3O_4/CoO	Ce^{4+}/Ce^{3+}
	Oα	Oβ	Oγ		
Co_8/ACs	16.2	68.6	15.2	0.87	–
Ce_8/ACs	18.2	68.5	13.3	–	3.83
Co_8Ce_3/ACs	21.7	65.8	12.5	0.94	2.98
Used Co_8Ce_3/ACs	15.6	51.9	32.5	2.35	4.12

major peaks shifted to lower temperature compared with Co_8/ACs and Ce_8/ACs, indicating that the interaction between Co and Ce oxides phases could enhance the mobility of active oxygen species on the surface and improve the reducibility [42], which was beneficial to removal activity of the catalyst. Meantime, the H_2-TPR analysis results were in line with the experiment result, which confirmed the addition of Ce played a great role in pollutant removal process.

3.5.3. XPS

XPS analysis was carried out to illuminate the valence states of the elements on the surface of the samples and to better elaborate the experimental removal mechanisms. The XPS O 1s spectra of the samples are shown in Fig. 10(a). And we can clearly see three peaks in all the samples, including peaks at lower binding energy value at 529.2–530.3 eV, which was assigned to the lattice oxygen(denoted as O_α), the one at around 531.3–532.3 eV corresponded to chemisorbed oxygen(denoted as O_β), and the peaks left at about 533.7 eV was attributed to hydroxyl groups or/and adsorbed water species (denoted as O_γ) [29,43]. The O_α, O_β and O_γ ratio of the samples were calculated by O_α/O_T, O_β/O_T and $O_\gamma/O_T(O_T = O_\alpha + O_\beta + O_\gamma)$, and the data are summarized in Table 2. In the four samples, the concentration of O_β is all highest, even its ratio more than 60% except Co_8Ce_3/ACs used sample. And it was reported that O_β was the most active species and had high mobility in oxidation reaction process [19]. From Fig. 10(a), we could see the ratio of O_α on Co_8Ce_3/ACs catalyst increased slightly and O_β reduced after modified with Co-Ce oxides, which was in line with the preceding statement. Moreover, most of all hydroxyl groups or/and adsorbed water species O_γ on the used Co_8Ce_3/ACs significantly enhanced, and the O_α, O_β all decreased to a certain extent. These results fully manifested that both lattice oxygen and chemisorbed oxygen participated in Hg^0 and HCHO removal process.

As seen from the Co 2p spectra in Fig. 10, the peaks at 781.4 eV and 797.3 eV were ascribed to Co_3O_4 phase, while the peaks at 786.2 eV and 803.4 eV were attributed to CoO phase for Co_8/ACs [22]. And when the sample was modified by CeO_2, the Co_3O_4/CoO ratio was improved from 0.87 to 0.94. And the fact indicated that the presence of CeO_2 may affect the oxidation state of cobalt, which was connected with the oxygen storage-release properties of ceria, therefore, some oxygen may combine with cobalt to form higher valence state [44]. From Fig. 10(b), the peaks existed slight deviation after the catalyst participated in the Hg^0 and HCHO removal process. This could be explained by the interaction between ceria and cobalt oxide during the reaction process. Besides, the ratio of Co_3O_4/CoO increased from 0.94 to 2.35 after Hg^0 and HCHO removal, indicating the oxidation of CoO occurred during the reaction process.

The XPS results of Ce 3d for three samples are shown in Fig. 10(c). The bands labeled as u were corresponding to Ce $3d_{3/2,}$ but those denoted as v were assigned to Ce $3d_{5/2}$. Among them, the u/v, u_2/v_2 and u_3/v_3 were assigned to the $3d^{10}4f^0$ state of Ce^{4+}, while the peaks labeled u_1/v_1 represented $3d^{10}4f^1$ state of Ce^{3+} [45]. There were a total of eight bands corresponding to Ce^{3+} and Ce^{4+} oxidation states on the all samples, of course, the Ce species was mainly in the form of CeO_2 on the surface of the catalysts. However, the peak area ratio of Ce^{4+}/Ce^{3+} reduced from 3.83 to 2.98 when cobalt oxide was introduced. According to reports, the presence of Ce^{3+} could charge imbalance, the vacancies and unsaturated chemical bonds on the surface of catalyst, resulting in more surface oxygen species formed [29]. And the fact was beneficial to the removal performances of Hg^0 and HCHO. In addition, the Ce^{4+}/Ce^{3+} ratio increased from 2.98 to 4.12 after removal, which further proved that the redox equilibrium of $Ce^{4+} + Co^{2+} \leftrightarrow Ce^{3+} + Co^{3+}$ occurred during the reaction process, and the fact was favorable to the removal efficiencies of Hg^0 and HCHO.

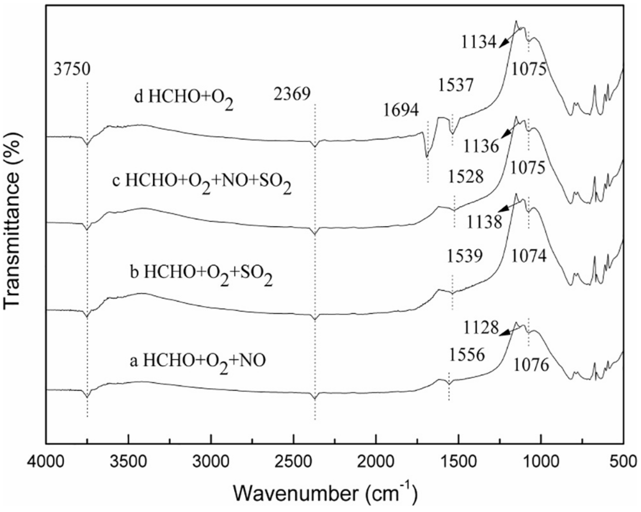

Fig. 11. FTIR spectra of Co_8Ce_3/ACs under different conditions: a.100 ppm HCHO + 6% O_2 + 350 ppm NO + N_2; b.100 ppm HCHO + 6% O_2 + 400 ppm SO_2 + N_2; c.100 ppm HCHO + 6% O_2 + 350 ppm NO + 400 ppm SO_2 + N_2. a-c were treated at ambient temperature. d. 100 ppm HCHO + 6% O_2 + N_2. d was treated at190 °C.

The XPS patterns of Hg 4f are shown in Fig. 10(d). The strong peak at 102.4 eV was attributed to characteristic peak of Si 2p [46], and the peak at around 104 eV was ascribed to HgO [47]. However, no adsorbed Hg^0 was detected on the surface of the catalyst, which may be due to the Hg^0 desorbed from the surface of the Co_8Ce_3/ACs catalyst or the too low concentration of adsorbed Hg^0. And the fact indicated HgO could be the main species on the surface of the catalyst during Hg^0 removal process, which corresponded to the experiment results.

3.5.4. FTIR

The FTIR spectra of Co_8Ce_3/ACs catalyst at different gases for 90 min are illustrated in Fig. 11. It could be clearly seen that the bands at 2369 cm^{-1} and 3750 cm^{-1} appeared in the four curves. The band at 3750 cm^{-1} could be assigned to the hydroxyl group on the surface of catalyst [48], which was beneficial for HCHO elimination. The band at 2369 cm^{-1} could be attributed to the stretching vibration of CO_2 [49]. Additionally, some bands between 500 and 1000 cm^{-1} in the Fig. 11 were assigned to Si-O, which were consistent with XRD results. In the curve of Fig. 11a, several weak bands at 3750, 2369, 1556, 1128, 1076 cm^{-1} were observed. The band at 1556 cm^{-1} demonstrated the formation of bidentate formate [50], and a band at 1128 cm^{-1} was attributed to bidentate nitrites, because of its poor thermal stability, leading to the formation of NO_2 [7]. As shown in Fig. 11b, a band at 1138 cm^{-1} was proposed to be the adsorbed sulfate [51]. For the curve of Fig. 11c, the two bands at 1136 and 1528 cm^{-1} could be assigned to gas-phase SO_2 [38] and NO_2-containing species, like nitrito(O-bound NO_2) and nitrato(NO_3) species [36] respectively. Besides, the bands at 3750, 2369, 1694, 1536, 1134, 1075 cm^{-1} were observed in the curve of Fig. 11d. According to previous report [52], the two bands at 1134 cm^{-1} and 1694 cm^{-1} were assigned to adsorbed molecular formaldehyde and the formic acid respectively. Moreover, the band at 1537 cm^{-1} was attributed to surface carbonate species [53]. On the basis of above results, we could know that a competition between NO, SO_2 and HCHO for active sites on the catalyst surface, meantime, the HCHO removal process was reasonably speculated.

3.6. Mechanisms discussion

On the basis of the above results about the experiments and characterizations, the possible reaction mechanisms of simultaneous removal of Hg^0 and HCHO over Co_8Ce_3/ACs catalyst were speculated. According to the results of XPS O1s, it could be seen that both the adsorbed oxygen (O_β) and lattice oxygen (O_α) involved in the reaction process. Meantime, both Co and Ce were able to shift between various oxidation states, which was proved by XPS Co2p and Ce3d. And the redox shift between Ce^{4+} and Ce^{3+} determined the oxygen storage capacity, which was significant for the consumed lattice oxygen. Of course, the adsorbed oxygen species on the catalyst could be replenished by capturing gas-phase oxygen molecules. To know the mercury species in the outlet gas, the results of mercury speciation conversion experiment were displayed in Fig. 6(b). The results demonstrated that a small part of mercury was captured by Co_8Ce_3/ACs catalyst, while most of the rest released into outlet flue gas as HgO form. According to the result analysis of XPS Hg4f and the Fig. 6(b) results, the possible mechanism of Hg^0 removal was proposed and the process was described as follow:

$$Hg^0(g) \rightarrow Hg^0(ad) \tag{5}$$

$$O_2 \rightarrow 2O_\beta \tag{6}$$

$$2CeO_2 \rightarrow Ce_2O_3 + O_\alpha \tag{7}$$

$$Co_3O_4 \rightarrow 3CoO + O_\alpha \tag{8}$$

$$2CeO_2 + 3CoO \rightarrow Ce_2O_3 + Co_3O_4(9) \tag{9}$$

$$Hg^0(ad) + O_\alpha \rightarrow HgO(ad) \tag{10}$$

$$Hg^0(ad) + O_\beta \rightarrow HgO(ad) \tag{11}$$

$$HgO(ad) \rightarrow HgO(g) \tag{12}$$

$$3CoO + 1/2O_2 \rightarrow Co_3O_4 \tag{13}$$

$$Ce_2O_3 + 1/2O_2 \rightarrow 2CeO_2 \tag{14}$$

What's more, combined with the stability test result and the results of FTIR and other characterization, the main gaseous products from HCHO removal reaction process was CO_2, and formate intermediate was observed in FTIR results. In this study, the HCHO removal was mainly attributed to the surface active oxygen species and hydroxyl radical on the catalyst surface, which were denoted as [O] and OH respectively. The consumed oxygen species on the catalyst could be replenished by capturing oxygen molecules, and the fast redox between Ce^{4+} and Ce^{3+} could be beneficial to the formation of the surface active oxygen species. Of course, the interaction between Co and Ce determined the catalytic property, which was conductive to the HCHO and Hg^0 removal. According to the existing results in the work and other researches [16], the HCHO removal process may be explained as follow:

$$HCHO(g) \rightarrow HCHO(ad) \tag{15}$$

$$2CeO_2 \rightarrow Ce_2O_3 + [O] \tag{16}$$

$$HCHO(ad) + [O] \rightarrow HCO + OH \tag{17}$$

$$HCO + OH \rightarrow HCOOH \tag{18}$$

$$Co_3O_4 + HCOOH \rightarrow 3CoO + HCOO + [O]^- + H^+ \tag{19}$$

$$HCOO\cdot + [O]^- \rightarrow HCO_3^- \tag{20}$$

$$HCO_3^- + H^+ \rightarrow CO_2(g) + H_2O(g) \tag{21}$$

$$Ce_2O_3 + 1/2O_2 \rightarrow 2CeO_2 \tag{22}$$

$$3CoO + 1/2O_2 \rightarrow Co_3O_4 \tag{23}$$

4. Conclusion

A series of CoCe/ACs catalysts showed more superior removal efficiencies of Hg^0 and HCHO than ACs, Co/ACs and Ce/ACs under the same conditions, among them, Co_8Ce_3/ACs exhibited the highest HCHO conversion (71.07%) and Hg^0 oxidation efficiency (69.43%) at 190 °C, and presented a certain stability for simultaneously removal of Hg^0 and HCHO during 60 h. The presence of Hg^0 had almost no influence on HCHO conversion, however, the addition of HCHO significantly reduced the Hg^0 oxidation. Besides, SO_2 had slight inhibitory effects on HCHO and Hg^0 removal, NO slightly reduced HCHO removal efficiency and promoted Hg^0 oxidation efficiency with the addition of 6% O_2 respectively. In addition, the characterization results showed that the features of Co_8Ce_3/ACs, such as the high dispersion of cobalt oxide, good texture properties, strong redox ability and the high active hydroxyl group, which were conductive to the HCHO and Hg^0 removal. However, the efficiencies of HCHO and Hg^0 simultaneous removal still remain to improve, of course, the regenerability of the Co_8Ce_3/ACs catalyst should be further studies in later day.

Acknowledgements

This work was financially supported by the National Nature Science Foundation of China (51478173), the National Key Research and Development Program of China (2016YFC0204100), and the Scientific and Technological Major Special Project of Changsha City in China (KQ1201011).

References

[1] F. Rezaei, A.A. Rownaghi, S. Monjezi, R.P. Lively, C.W. Jones, SOx/NOx Removal from flue gas streams by solid adsorbents: a review of current challenges and future directions, Energy Fuels 29 (2015) 5467–5486.

[2] H. Li, L. Zhu, J. Wang, L. Li, K. Shih, Development of nano-sulfide sorbent for efficient removal of elemental mercury from coal combustion fuel gas, Environ. Sci. Technol. 50 (2016) 9551–9557.

[3] I. Gulyurtlu, P. Abelha, A. Gregóri, A. García-García, D. Boavida, A. Crujeira, I. Cabrita, The emissions of VOCs during Co-combustion of coal with different waste materials in a fluidized bed, Energy Fuels 18 (2004) 605–610.

[4] J.H. Pavlish, E.A. Sondreal, M.D. Mann, E.S. Olson, K.C. Galbreath, D.L. Laudal, S.A. Benson, Status review of mercury control options for coal-fired power plants, Fuel Process. Technol. 82 (2003) 89–165.

[5] X. Huang, M. Li, H.R. Friedli, Y. Song, D. Chang, L. Zhu, Mercury emissions from biomass burning in China, Environ. Sci. Technol. 45 (2011) 9442–9448.

[6] J.P. Garcia, S. Beyne-Masclet, G. Mouvier, Emissions of volatile organic compounds by coal-fired power stations, Atmos. Environ. 26 (1992) 1589–1597.

[7] J. Sheng, C. Li, L. Zhao, X. Du, L. Gao, G. Zeng, Efficient removal of HCHO from simulated coal combustion flue gas using CuO-CeO_2 supported on cylindrical activated coke, Fuel 197 (2017) 397–406.

[8] S. Lu, K. Li, F. Huang, C. Chen, B. Sun, Efficient MnOx-Co_3O_4-CeO_2 catalysts for formaldehyde elimination, Appl. Surf. Sci. 400 (2017) 277–282.

[9] Z. Fan, Z. Zhang, W. Fang, X. Yao, G. Zou, W. Shangguan, Low-temperature catalytic oxidation of formaldehyde over Co_3O_4 catalysts prepared using various precipitants, Chin. J. Catal. 37 (2016) 947–954.

[10] B. Bai, Q. Qiao, J. Li, J. Hao, Progress in research on catalysts for catalytic oxidation of formaldehyde, Chin. J. Catal. 37 (2016) 102–122.

[11] J. Yang, Y. Zhao, S. Ma, B. Zhu, J. Zhang, C. Zheng, Mercury Removal by Magnetic Biochar Derived from Simultaneous Activation and Magnetization of Sawdust, Environ. Sci. Technol. 50 (2016) 12040–12047.

[12] S. Zhao, Y. Duan, T. Yao, M. Liu, J. Lu, H. Tan, X. Wang, L. Wu, Study on the mercury emission and transformation in an ultra-low emission coal-fired power plant, Fuel 199 (2017) 653–661.

[13] Z. Zhou, X. Liu, Z. Liao, H. Shao, Y. Hu, Y. Xu, M. Xu, A novel low temperature catalyst regenerated from deactivated SCR catalyst for Hg^0 oxidation, Chem. Eng. J. 304 (2016) 121–128.

[14] S. Tao, C. Li, X. Fan, G. Zeng, P. Lu, X. Zhang, Q. Wen, W. Zhao, D. Luo, C. Fan, Activated coke impregnated with cerium chloride used for elemental mercury removal from simulated flue gas, Chem. Eng. J. 210 (2012) 547–556.

[15] Y. Gao, Z. Zhang, J. Wu, L. Duan, A. Umar, L. Sun, Z. Guo, Q. Wang, A critical review on the heterogeneous catalytic oxidation of elemental mercury in flue gases, Environ. Sci. Technol. 47 (2013) 10813–10823.

[16] X. Zhu, X. Gao, R. Qin, Y. Zeng, R. Qu, C. Zheng, X. Tu, Plasma-catalytic removal of formaldehyde over Cu–Ce catalysts in a dielectric barrier discharge reactor, Appl. Catal. B 170–171 (2015) 293–300.

[17] Z. Xu, J. Yu, M. Jaroniec, Efficient catalytic removal of formaldehyde at room temperature using AlOOH nanoflakes with deposited Pt, Appl. Catal. B 163 (2015)

306–312.
[18] C. Zhang, H. He, K.-I. Tanaka, Catalytic performance and mechanism of a Pt/TiO_2 catalyst for the oxidation of formaldehyde at room temperature, Appl. Catal. B 65 (2006) 37–43.
[19] H. Li, C.Y. Wu, Y. Li, J. Zhang, CeO_2-TiO_2 catalysts for catalytic oxidation of elemental mercury in low-rank coal combustion flue gas, Environ. Sci. Technol. 45 (2011) 7394–7400.
[20] M. Wang, L. Zhang, W. Huang, T. Xiu, C. Zhuang, J. Shi, The catalytic oxidation removal of low-concentration HCHO at high space velocity by partially crystallized mesoporous MnOx, Chem. Eng. J. 320 (2017) 667–676.
[21] B. Bai, H. Arandiyan, J. Li, Comparison of the performance for oxidation of formaldehyde on nano-Co_3O_4, 2D-Co_3O_4, and 3D-Co_3O_4 catalysts, Appl. Catal. B 142–143 (2013) 677–683.
[22] H. Wu, C. Li, L. Zhao, J. Zhang, G. Zeng, Y.E. Xie, X. Zhang, Y. Wang, Removal of gaseous elemental mercury by cylindrical activated coke loaded with CoOx-CeO_2 from simulated coal combustion flue gas, Energy Fuels 29 (2015) 6747–6757.
[23] Y. Liu, Y. Wang, H. Wang, Z. Wu, Catalytic oxidation of gas-phase mercury over Co/TiO_2 catalysts prepared by sol–gel method, Catal. Commun. 12 (2011) 1291–1294.
[24] Z. Mei, Z. Shen, Q. Zhao, W. Wang, Y. Zhang, Removal and recovery of gas-phase element mercury by metal oxide-loaded activated carbon, J. Hazard. Mater. 152 (2008) 721–729.
[25] A. Zhang, W. Zheng, J. Song, S. Hu, Z. Liu, J. Xiang, Cobalt manganese oxides modified titania catalysts for oxidation of elemental mercury at low flue gas temperature, Chem. Eng. J. 236 (2014) 29–38.
[26] C. Shi, Y. Wang, A. Zhu, B. Chen, C. Au, $MnxCo_{3-x}O_4$ solid solution as high-efficient catalysts for low-temperature oxidation of formaldehyde, Catal. Commun. 28 (2012) 18–22.
[27] L. Bai, F. Wyrwalski, M. Safariamin, R. Bleta, J.-F. Lamonier, C. Przybylski, E. Monflier, A. Ponchel, Cyclodextrin-cobalt (II) molecule-ion pairs as precursors to active Co_3O_4/ZrO_2 catalysts for the complete oxidation of formaldehyde: Influence of the cobalt source, J. Catal. 341 (2016) 191–204.
[28] J. Ma, C. Li, L. Zhao, J. Zhang, J. Song, G. Zeng, X. Zhang, Y. Xie, Study on removal of elemental mercury from simulated flue gas over activated coke treated by acid, Appl. Surf. Sci. 329 (2015) 292–300.
[29] L. Zhao, C. Li, S. Li, Y. Wang, J. Zhang, T. Wang, G. Zeng, Simultaneous removal of elemental mercury and NO in simulated flue gas over V_2O_5 /ZrO_2-CeO_2 catalyst, Appl. Catal. B 198 (2016) 420–430.
[30] L. Xue, C. Zhang, H. He, Y. Teraoka, Catalytic decomposition of N_2O over CeO_2 promoted Co_3O_4 spinel catalyst, Appl. Catal. B 75 (2007) 167–174.
[31] L.F. Liotta, G. Di Carlo, G. Pantaleo, A.M. Venezia, G. Deganello, Co_3O_4/CeO_2 composite oxides for methane emissions abatement: Relationship between Co_3O_4–CeO_2 interaction and catalytic activity, Appl. Catal. B 66 (2006) 217–227.
[32] B. Zhao, H. Yi, X. Tang, Q. Li, D. Liu, F. Gao, Copper modified activated coke for mercury removal from coal-fired flue gas, Chem. Eng. J. 286 (2016) 585–593.
[33] H. Li, C.Y. Wu, Y. Li, L. Li, Y. Zhao, J. Zhang, Role of flue gas components in mercury oxidation over TiO_2 supported MnOx-CeO_2 mixed-oxide at low temperature, J. Hazard. Mater. 243 (2012) 117–123.
[34] S. Zhang, Y. Zhao, Z. Wang, J. Zhang, L. Wang, C. Zheng, Integrated removal of NO and mercury from coal combustion flue gas using manganese oxides supported on TiO_2, J. Environ. Sci. 53 (2017) 141–150.
[35] H. Li, S. Wang, X. Wang, N. Tang, S. Pan, J. Hu, Catalytic oxidation of Hg^0 in flue gas over Ce modified TiO_2 supported Co-Mn catalysts: Characterization, the effect of gas composition and co-benefit of NO conversion, Fuel 202 (2017) 470–482.
[36] R. Jin, Y. Liu, Z. Wu, H. Wang, T. Gu, Low-temperature selective catalytic reduction of NO with NH(3) over Mn-Ce oxides supported on TiO_2 and Al_2O_3: a comparative study, Chemosphere 78 (2010) 1160–1166.
[37] A. Fuente-Cuesta, M.A. Lopez-Anton, M. Diaz-Somoano, M.R. Martínez-Tarazona, Retention of mercury by low-cost sorbents: Influence of flue gas composition and fly ash occurrence, Chem. Eng. J. 213 (2012) 16–21.
[38] J. Zhang, C. Li, L. Zhao, T. Wang, S. Li, G. Zeng, A sol-gel Ti-Al-Ce-nanoparticle catalyst for simultaneous removal of NO and Hg^0 from simulated flue gas, Chem. Eng. J. 313 (2017) 1535–1547.
[39] P. Yang, S. Yang, Z. Shi, Z. Meng, R. Zhou, Deep oxidation of chlorinated VOCs over CeO_2-based transition metal mixed oxide catalysts, Appl. Catal. B 162 (2015) 227–235.
[40] L. Wang, X. Cheng, Z. Wang, C. Ma, Y. Qin, Investigation on Fe-Co binary metal oxides supported on activated semi-coke for NO reduction by CO, Appl. Catal. B 201 (2017) 636–651.
[41] J. Wang, M. Shen, J. Wang, J. Gao, J. Ma, S. Liu, CeO_2–CoOx mixed oxides: Structural characteristics and dynamic storage/release capacity, Catal. Today 175 (2011) 65–71.
[42] M. Zabilskiy, B. Erjavec, P. Djinović, A. Pintar, Ordered mesoporous CuO–CeO_2 mixed oxides as an effective catalyst for N_2O decomposition, Chem. Eng. J. 254 (2014) 153–162.
[43] H. Huang, P. Hu, H. Huang, J. Chen, X. Ye, D.Y.C. Leung, Highly dispersed and active supported Pt nanoparticles for gaseous formaldehyde oxidation: influence of particle size, Chem. Eng. J. 252 (2014) 320–326.
[44] J. Luo, M. Meng, X. Li, X. Li, Y. Zha, T. Hu, Y. Xie, J. Zhang, Mesoporous Co_3O_4–CeO_2 and Pd/Co_3O_4–CeO_2 catalysts: Synthesis, characterization and mechanistic study of their catalytic properties for low-temperature CO oxidation, J. Catal. 254 (2008) 310–324.
[45] Z. Zhou, X. Liu, Z. Liao, H. Shao, C. Lv, Y. Hu, M. Xu, Manganese doped CeO $_2$-ZrO_2 catalyst for elemental mercury oxidation at low temperature, Fuel Process. Technol. 152 (2016) 285–293.
[46] Y. Wang, B. Shen, C. He, S. Yue, F. Wang, Simultaneous Removal of NO and Hg(0) from Flue Gas over Mn-Ce/Ti-PILCs, Environ. Sci. Technol. 49 (2015) 9355–9363.
[47] C. He, B. Shen, J. Chen, J. Cai, Adsorption and oxidation of elemental mercury over Ce-MnOx/Ti-PILCs, Environ. Sci. Technol. 48 (2014) 7891–7898.
[48] D.W. Kwon, P.W. Seo, G.J. Kim, S.C. Hong, Characteristics of the HCHO oxidation reaction over Pt/TiO_2 catalysts at room temperature: The effect of relative humidity on catalytic activity, Appl. Catal. B 163 (2015) 436–443.
[49] L. Qi, B. Cheng, J. Yu, W. Ho, High-surface area mesoporous Pt/TiO(2) hollow chains for efficient formaldehyde decomposition at ambient temperature, J. Hazard. Mater. 301 (2016) 522–530.
[50] E.A. Ivanov, G.Y. Popova, Y.A. Chesalov, T.V. Andrushkevich, In situ FTIR study of the kinetics of formic acid decomposition on V-Ti oxide catalyst under stationary and non-stationary conditions, Determination of kinetic constants, J. Mol. Catal. A: Chem. 312 (2009) 92–96.
[51] L. Zhao, X. Li, X. Quan, G. Chen, Effects of surface features on sulfur dioxide adsorption on calcined NiAl hydrotalcite-like compounds, Environ. Sci. Technol. 45 (2011) 5373–5379.
[52] J.T. Kecskés, J.K. Raskó, FTIR and mass spectrometric studies on the interaction of formaldehyde with TiO_2 supported Pt and Au catalysts, Appl. Catal. A 273 (2004) 55–62.
[53] Y. Wang, X. Zhu, M. Crocker, B. Chen, C. Shi, A comparative study of the catalytic oxidation of HCHO and CO over $Mn_{0.75}Co_{2.25}O_4$ catalyst: The effect of moisture, Appl. Catal. B 160–161 (2014) 542–551.